MECHANIKA TEORETYCZNA
I STOSOWANA
Journal of Theoretical
and Applied Mechanics
2, 34, 1996

THE EVOLUTION OF KINEMATIC AND ISOTROPIC HARDENING IN THE CASE OF COMPLEX UNIAXIAL LOADING

EWA SENDER

WIESŁAW TRĄMPCZYŃSKI

Institute of Fundamental Technological Research, Warsaw

e-mail: wtramp@ippt.gov.pl

This paper is concerned with uniaxial behaviour of four different construction steels in the plastic range. A set of monotonic and cyclic loading (tension-compression) experiments was conducted on round bar specimens made 18G2A, St3s, 40H and 45 steel at room temperature. First two materials show cyclic hardening but different behaviour in the case of monotonic loading (large and small plasticity knee) and the last two ones show cyclic softening. Results concerning monotonic loading, strain controlled symmetric cyclic loading and stress-controlled non-symmetric cyclic loading (ratchetting) are presented. All experiments were performed on similar specimens, the same laboratory equipment and using the same experimental technique.
Using the "two point" technique of successive unloadings, the standard physical quantities and the stress jumps corresponding to the opposite direction of plastic straining were measured. For the Huber-Mises yield surface such data enable to follow the evolution of kinematic and isotropic hardening.

1. Introduction

Since quite a lot of structures are designed to withstand complex loading, including plastic one, it is quite important to collect wide spectrum of experimental data, specially for complex loading conditions. They can be used as a *tool for the material behaviour prediction and for constitutive model testing* and modification.

Although quite a lot of experimental programs in this field have been carried out since a long time (cf Landgraf (1969); Jhansale (1975); Śliwowski

(1979); Ohashi et al. (1985); Benallal and Marquis (1987); Ohnami et al. (1988); Ishikawa and Sasaki (1989); Hassan and Kyriakides (1992); Hassan et al. (1992); Sender and Trąmpczyński (1995); Lehmann et al. (1985); Kowalewski (1994)) there is still lack of consistent data for wider range of materials, obtained using this same equipment, specimens and experimental technique. It concerns also the complex uniaxial loading histories, since some effects observed experimentally for such loading conditions are not still described even by modern theoretical description (cf Rodzik (1993); Chaboche (1975)). The evolution of the yield surface parameters due to complex plastic histories can be mentioned as an example (cf Sender et al. (1995)). Hence, it is quite important to collect experimental data, even for uniaxial loading conditions, since majority of the proposed theories are based on the idea of kinematic and isotropic hardening.

In this paper the results of complex uniaxial loading program for 18G2A, St3s, 40H and 45 steel are presented and discussed on the basis of the stress-strain relation and the yield surface parameters evolution. The yield surface parameters evolution due to different loading histories were determined using the "two-point" unloading technique.

Although realized experimental program is similar to that described by Sender and Trąmpczyński (1995) for 18G2A steel, in this paper the results for four different types of construction steel are presented and the following effects are compared:

- The evolution of kinematic and isotropic hardening for monotonic and cyclic loading
- Memory of maximal prestress (cyclic and monotonic one)
- Material behaviour in the range of ratchetting loading (only for 18G2A and 40H steel).

It is shown that although examined materials exhibit different specific behaviour, the main effects are of the similar nature.

The "two-point" unloading technique was precisely described by Lehmann et al. (1985) and Trąmpczyński (1989) in Fig.1 it is explained in the case of uniaxial loading. Let us assume the basic program of plastic straining O-A. The loading is interrupted at the point A - σ_a (the stress deviator at this point is S_{ij}), specimen is unloaded and then reloaded into reverse straining direction until the small value of the increment of $\eta = \varepsilon_x^p$ (the yield definition) is achieved. The end of the stress deviator S_{ij}^R lies on the yield surface, where the plastic strain-rate vector has the direction opposite to that prescribed in

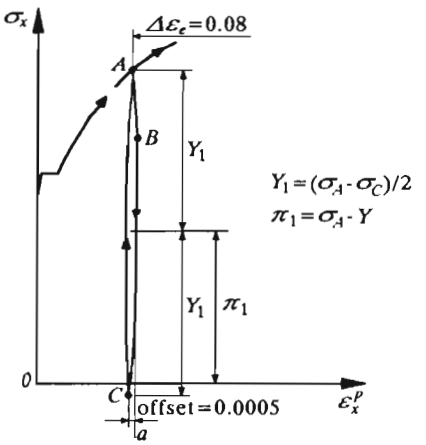

Fig. 1. Application of the two points technique in the case of monotonic tension

the basic program. At this moment (point $C - \sigma_c$) the reloading process is stopped, the specimen is unloaded and loaded in the former direction. The basic straining program is then continued. In this way two well defined points S_{ij} (σ_a) and S_{ij}^R (σ_c) on the current yield surface are obtained, for the chosen plastic strain history (it is assumed that the plastic strain increment due to the yield definition is negligible). The first point lies on the yield surface where the plastic strain rate vector has the direction prescribed by the basic program, and the second one lies on the yield surface where the plastic strain rate vector has the opposite direction. Even for quite complex loading (e.g. cyclic ones), the evolution of such parameters as $\pi_1 = (\sigma_a + \sigma_c)/2$ and $Y_1 = (\sigma_a - \sigma_c)/2$ can be followed this way. In the case of Huber-Mises yield surface (cf Lehmann et al. (1985)), π_1 and Y_1 parameters denote the yield surface centre position $(\pi_1 = \alpha)$ and its radius $(Y_1 = R)$, respectively.

2. Experimental procedure

The experimental programs were performed on solid circular specimens at room temperature. The specimen dimensions: diameter $D = 12$ m (for 18G2A and St3s steel) and $D = 9$ mm (for 40H and 45 steel), specimen gauge length $L = 15$ mm were chosen experimentally and then verified theoretically using the FEM program ABAQUS. Tension-compression cyclic programs were ccarried out using a closed-loop servo-hydraulic Instron 8501 uniaxial machine.

Force acting upon the specimen and its elongation were read by a computer, elaborated and the results obtained were used for continuous machine control. The longest time of information path: machine-computer-machine of the program used was 0.05 s. All programs were performed with a constant plastic strain rate $\dot{\varepsilon}_x^p = 3.4 \cdot 10^{-4}\,\mathrm{s}^{-1}$ and the actual stress versus the logarithmic plastic strain were calculated and plotted ($\varepsilon = \ln(l/l_0)$, $\sigma = P/F_a$, where l_0 – gauge length, F_a – current specimen cross-section, P – force). The yield points were defined by the offset definition $\eta = 0.0005$ in a way described by Lehmann et al. (1985) and Trąmpczyński (1989).

3. Experimental results

Although quite extensive experimental program for four different types of steel was carried out, only the most typical data for chosen materials, are presented in this paper as an example. It was found that experimental results for two hardening materials (18G2A and St3s steel) are qualitatively quite similar as well as results for two softening materials (40H and 45 steel). Because the presented experimental program is similar to that described by Sender and Trąmpczyński (1995) for 18G2A steel, mainly data for materials showing cyclic softening are presented as an example.

3.1. Monotonic tension (with unloading)

The specimens were loaded by tension at the constant plastic strain rate $\dot{\varepsilon}_x^p = 3.4 \cdot 10^{-4}\,\mathrm{s}^{-1}$. After every chosen plastic strain increment $\Delta\varepsilon_x^p$ the π and Y_1 values were determined using the "two point" unloading technique. The loading paths for stress σ, π_1 and Y_1 are shown in Fig.2 and Fig.3 taking as an example the 18G2A and 40H steel behaviour.

For all materials, the parameter π_1, shows similar qualitative behaviour and continually increases its value.

In the case of 18G2A and St3s steel, the parameter Y_1 initially decreases, then increases and saturates at plastic strains $\varepsilon_x^p \approx 0.1$. Further material hardening is caused by increasing the π_1 value only (Fig.2).

In the case of 40H and 45 steel, the parameter Y_1 continually decreases (Fig.3).

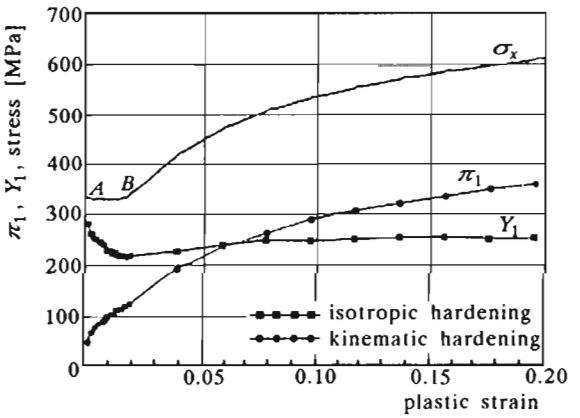

Fig. 2. Monotonic tension for 18G2A steel

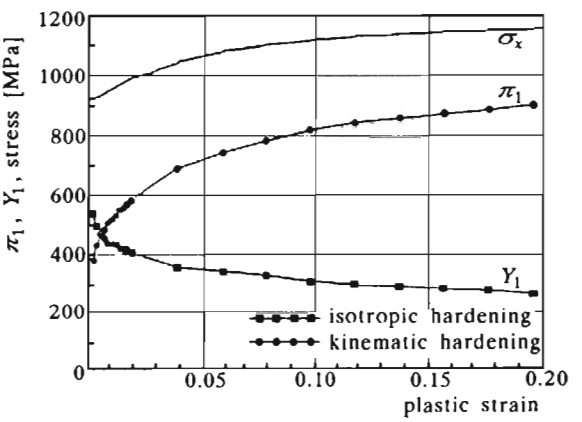

Fig. 3. Monotonic tension for 40H steel

In all cases, within the yield knee range (for example Fig.2 AB) two simultaneous processes are observed: increase of parameter π_1 and decrease of parameter Y_1.

3.2. Strain-controlled cyclic tension-compression (with unloading) – cyclic amplitude memory effect

The specimens were loaded by cyclic tension-compression with constant

strain amplitude: $\varepsilon_x^p = \pm 0.02$ for 18G2A and St3s steel and $\varepsilon_x^p = \pm 0.015$ for 40H and 45 steel. Using the "unloading technique" the variations of parameters π_1 and Y_1 were determined from the beginning up to the stabilised loop. In Fig.4 the stress-strain, π_1 and Y_1 curves are presented in the case of 40H steel as an example. Solid line shows the first three half-cycles, and the dashed one shows the stabilised loop.

18G2A and St3s steel exhibits cyclic hardening, the major part of which occurs during the first three half-cycles (both for π_1 and for Y_1). The general shape of the π_1 path changes during the first three half-cycles, and then remains constant at the steady state being similar to the stress-strain curve. In the steady state the parameter Y_1 remains constant.

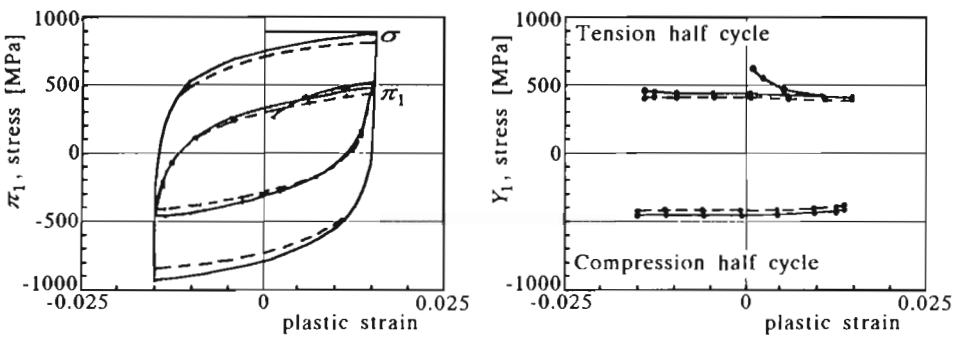

Fig. 4. Cyclic tension-compresion loading with constant strain amplitude (40H steel $\varepsilon_x^p \pm 0.015$)

40H and 45 steel (Fig.4) exhibits cyclic softening as well for π_1 and Y_1 values. As before the major part of this effect occurs during the first three half-cycles. The general shape of the π_1 path remains almost unchanged at the steady state being similar to the stress-strain curve. In the steady state cycles the parameter Y_1 remains constant.

In Fig.5 the skeleton curves for stress σ, π_1 and Y_1 in the case of increasing strain amplitudes (solid line) are compared with those for decreasing strain amplitudes (dashed line) taking as an example the 45 steel behaviour. The proper monotonic tension curves for stress, π_1 and Y_1 are also shown for comparison.

In the case of 18G2A and St3s steel, there were two experimental programs, consisting of the following growing and decreasing amplitudes: $\varepsilon_x^p = \pm 0.005$, 0.01, 0.015, 0.02; $\varepsilon_x^p = \pm 0.02$, 0.015, 0.010, 0.05. For 40H and 45 steel it was the following amplitudes sequence: $\varepsilon_x^p = \pm 0.004$, 0.007, 0.010, 0.015 and $\varepsilon_x^p = \pm 0.015$, 0.010, 0.007, 0.004.

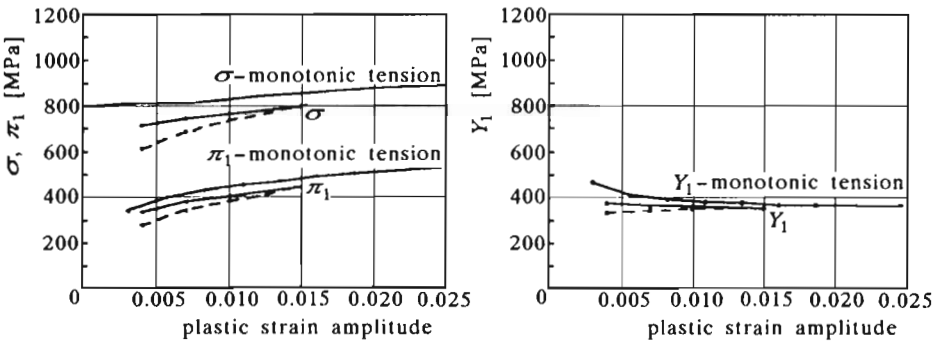

Fig. 5. σ, π_1 and Y_1 skeleton points for increasing strain amplitudes (solid line – $\varepsilon_x^p = \pm 0.004, 0.007, 0.010, 0.015$) and decreasing strain amplitudes (dashed line – $\varepsilon_x^p = \pm 0.015, 0.010, 0.007, 0.004$) in the case of 45 steel

The values of π_1 and Y_1 for cyclic amplitude $\varepsilon_x^p = \pm 0.02$ ($\varepsilon_x^p = \pm 0.015$) for a virgin material are the same as for the material with the history of increasing amplitudes. It means that cyclic loading history with smaller amplitudes has no influence on the material cyclic behaviour with higher amplitudes. Difference between the solid and dashed lines indicates the influence of the cyclic *loading history with higher amplitudes on the material behaviour under cyclic* loading with smaller amplitudes.

In the case of materials showing cyclic hardening (18G2A and St3s steel) this memory manifests as higher skeleton point values (for π_1 and Y_1 parameters) then those for a virgin material. For materials showing cyclic softening (40H and 45 steel) such memory manifests as lower skeleton points values (Fig.5).

Memory of maximal prestress is included mainly in behaviour of the π_1 parameter in the case of 18G2A steel. In the case of St3s, 40H and 45 steel the memory effect is included as well in behaviour of the π_1 as in Y_1 parameters.

3.3. Strain-controlled cyclic tension-compression (with unloading) after monotonic prestrain – memory of monotonic prestrain

The specimens were plastically prestrained up to $\varepsilon_x^p = 0.092$ and then cyclically loaded with plastic strain amplitude: $\varepsilon_x^p = \pm 0.005$ for 18G2A and St3s steel and strain amplitude $\varepsilon_x^p = \pm 0.004$ for 40H and 45 steel. The stress-strain, π_1 and Y_1 cyclic curves for 40H steel are presented in Fig.6, as an example.

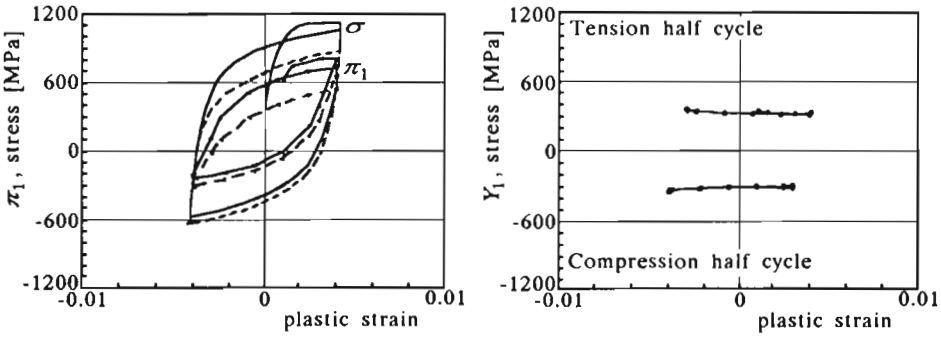

Fig. 6. Cyclic tension-compresion loading ($\varepsilon_x^p = \pm 0.004$) with constant strain amplitude after prestrain by monotonic tension $\varepsilon_x^p = \pm = 0.092$ for 40H steel

After hardening caused by plastic prestrain, cyclic relaxation of stresses σ and π_1 is observed mainly in the prestrain direction. Even after many cycles the stress and π_1 values at the prestrained direction do not relax to the corresponding values in the "opposite direction" and steady cycle remains non-symmetric. Quite symmetric behaviour of Y_1 is observed from the very beginning.

The similar program, where monotonic prestrain $\varepsilon_x^p = 0.092$ was followed by cyclic loading with plastic strain amplitude: $\varepsilon_x^p = \pm 0.015$ for 18G2A and St3s steel and $\varepsilon_x^p = \pm 0.010$ for 40H and 45 steel was then performed and its results are presented in Fig.7, where the stress-strain, π_1 and Y_1 cyclic curves for 40H steel are shown as an example.

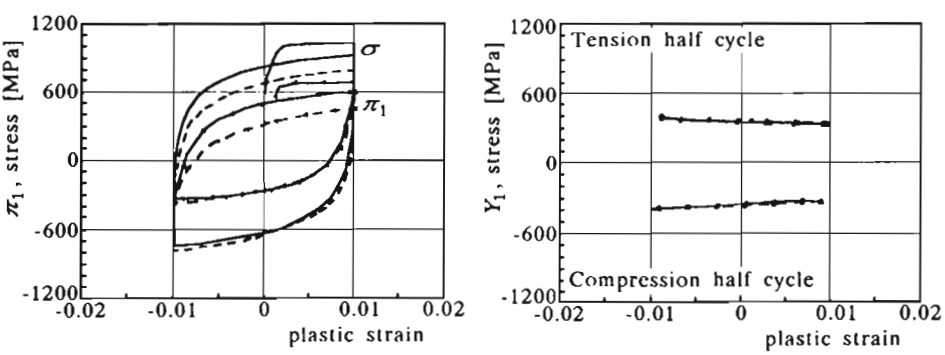

Fig. 7. Cyclic tension-compresion loading ($\varepsilon_x^p = \pm 0.010$) with constant strain amplitude after prestrain by monotonic tension $\varepsilon_x^p = 0.092$ for 40H steel

As before, after hardening caused by plastic prestrain, cyclic relaxation

of stresses σ and π_1, but mainly in the prestrain direction, is observed. In the direction opposite to the prestrain, the shapes of the stress-strain and the π_1 curves remain almost unchanged from the beginning. After several cycles, a steady cycle becomes nearly symmetric. Y_1 remains constant from the beginning.

3.4. The influence of complex plastic prestrain loading on material behaviour under monotonic loading

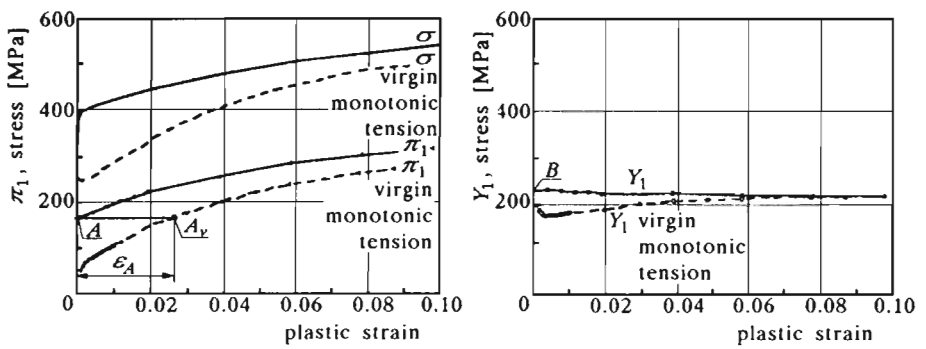

Fig. 8. St3s steel monotonic tension after following complex plastic strain history: – monotonic prestrain $\varepsilon_x^p = 0.092$ followed by cyclic loading with the plastic strain amplitudes: $\varepsilon_x^p = \pm 0.015, \pm 0.01, \pm 0.005, \pm 0.015$

The specimens were plastically prestrained by two types of complex loading histories:

I – Monotonic prestrain $\varepsilon_x^p = 0.092$ followed by cyclic loading with the plastic strain amplitudes: $\varepsilon_x^p \pm 0.015, \pm 0.01, \pm 0.005, \pm 0.015$ for 18G2A and St3s steel (Fig.8)

II – Cyclic loading with the following plastic strain amplitudes: $\varepsilon_x^p = \pm 0.005$, $\pm 0.01, \pm 0.015, \pm 0.02$ for 18G2A and St3s steel

I – Monotonic prestrain $\varepsilon_x^p = 0.092$ followed by cyclic loading with the plastic strain amplitudes: $\varepsilon_x^p = \pm 0.01, \pm 0.007, \pm 0.004, \pm 0.01$ for 40H and 45 steel (Fig.9a)

II – Cyclic loading with the following plastic strain amplitudes: $\varepsilon_x^p = \pm 0.005$, $\pm 0.01, \pm 0.015, \pm 0.02$ for 40H and 45 steel (Fig.9b).

and then monotonically tensioned.

The stress-strain, π_1 and Y_1 monotonic tension curves for St3s and 45 steel, after such prestrain, are shown in Fig.8 and Fig.9 (solid lines) as an example. The virgin material monotonic tension curves are also presented for comparison (dashed lines).

In the case of 18G2A and St3s steel (Fig.8) the π_1 value continuously increases and the parameter Y_1 is almost constant.

In the case of 40H and 45 steel (Fig.9a,b), π_1 value increases in a way similar to that for virgin specimen monotonic loading (dashed line) and the parameter Y_1 decreases.

Let us assume, for simplicity, that in the case of virgin material monotonic loading (Fig.8 and Fig.9 – dashed line)

$$\sigma = \pi_1 + Y_1 \qquad \pi_1 = f_1(\varepsilon^p) \qquad Y_1 = f_2(\varepsilon^p) \tag{3.1}$$

(in the case of 18G2A and St3s steel only the convex part of Y_1 – plastic strain curve was approximated – Fig.8) and refer $\pi_1^h = A$ and $Y_1^h = B$ values resulted from the former complex plastic strain history to the virgin material monotonic loading curves (Fig.8 $A \to A_v$; Fig.9a,b $B \to B_v$)

$$\pi_1^h = A = f_1(\varepsilon_A) \qquad Y_1^h = B = f_2(\varepsilon_B) \tag{3.2}$$

In the case of 18G2A and St3s steel (Fig.8) the monotonic loading, following a complex plastic strain history resulted with $\pi_1 = A$ and $Y_1 = B$ values, can be described by the equations

$$\begin{aligned} &\sigma = \pi_1 + Y_1 && \pi_1 = f_1(\varepsilon^p + \varepsilon_A) \\ &Y_1 = f_2(\varepsilon^p + \varepsilon_B) && \text{for } B < Y_c \\ &Y_1 = B && \text{for } B \geq Y_c \end{aligned} \tag{3.3}$$

where Y_c denote Y_1 uniaxial tension asymptotic value.

In the case of 40H and 45 steel (Fig.9) Eq (3.3) takes the following form

$$\sigma = \pi_1 + Y_1 \qquad \pi_1 = f_1(\varepsilon^p) - C \qquad Y_1 = f_2(\varepsilon^p + \varepsilon_B) \tag{3.4}$$

where $C \geq 0$ value represents the complexity of prestrain history.

Comparison between experimental stress-plastic strain data for monotonic tension after complex plastic strain history (dashed line – 45 steel; history I) and data calculated in the way described above (Eq (3.4) – solid line) is presented in Fig.9c.

Quite good prediction means, that influence of even complex plastic prestrain history on following monotonic loading can be described only by $\pi_1 = A$ and $Y_1 = B$ values resulted from the former complex plastic strain history. In the case of 40H and 45 steel, the value of C has to be taken into account.

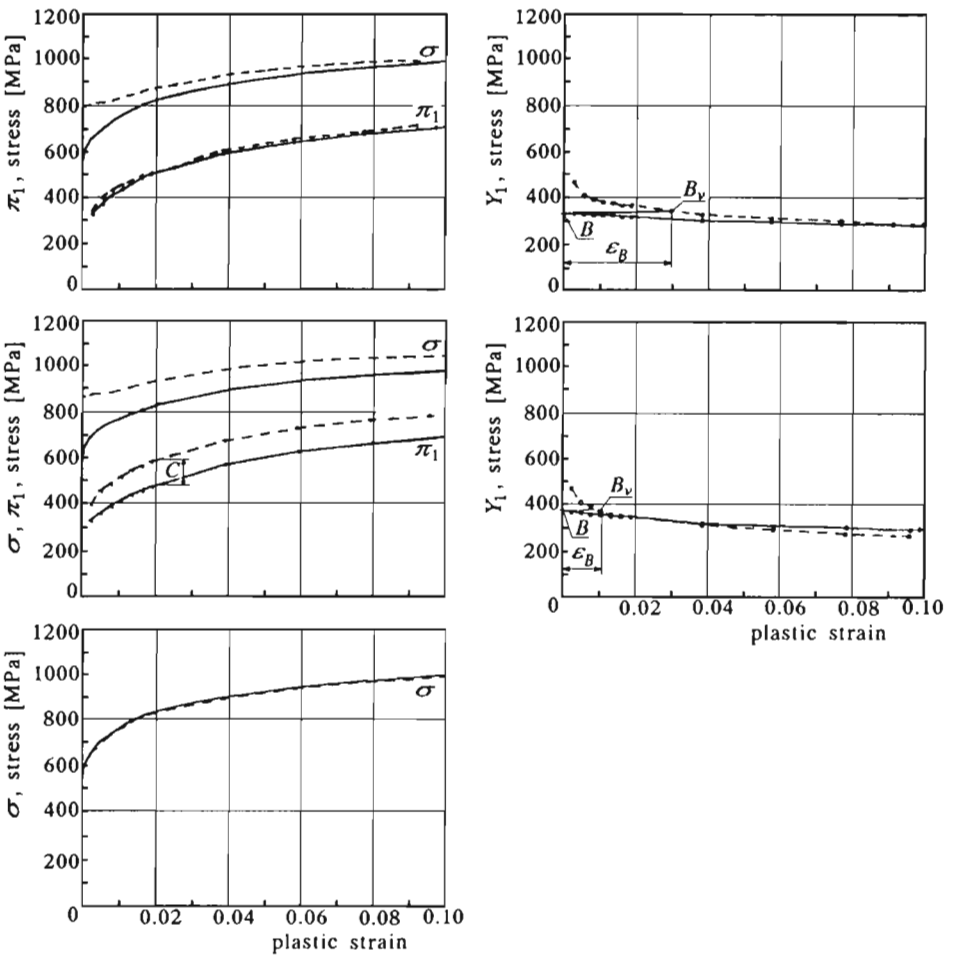

Fig. 9. 45 steel monotonic tension after complex plastic strain histories: (a) – monotonic prestrain $\varepsilon_x^p = 0.092$ followed by cyclic loading with the plastic strain amplitudes: $\varepsilon_x^p = \pm 0.01, \pm 0.007, \pm 0.004, \pm 0.01$; (b) – cyclic loading with the strain amplitudes $\varepsilon_x^p = \pm 0.004, \pm 0.007, \pm 0.01, \pm 0.015$; (c) – comparison between experimental stress-strain data for monotonic tension after complex plastic strain history (dashed line – Fig.9a) and calculated (solid line – Eq (3.4)) results

3.5. Stress-controlled cyclic tension-compression (ratchetting)

The ratchetting phenomenon corresponds to the progressive distortion, cycle-by-cycle, induced by superposition of a primary loading (considered as constant) and a secondary cyclic loading. Under uniaxial conditions, the mean stress σ_m can be considered as the "primary load" and the cyclic stress (amplitude σ_a) as the secondary one. The ratchetting parameters used in this paper

$$\sigma_m = \frac{\sigma_{\max} + \sigma_{\min}}{2} \qquad \sigma_a = \sigma_{\max} - \sigma_m$$

$\delta\varepsilon_r^p$ – one cycle ratchetting strain
$\delta\varepsilon_r^{ps}$ – one cycle ratchetting strain at steady state
ε_r^p – ratchetting strain after N cycles
are presented in Fig.10.

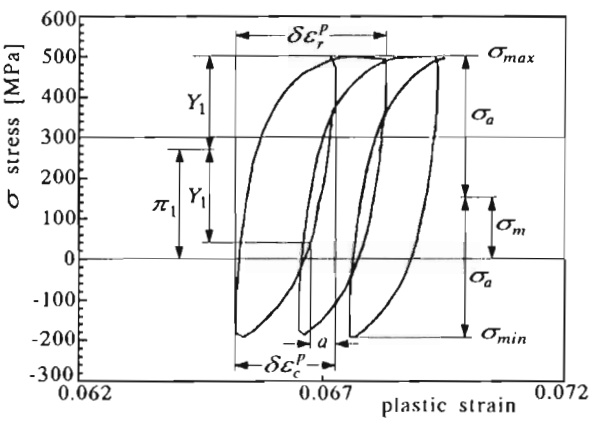

Fig. 10. Main ratchetting parameters

Results of an extensive ratchetting strain program for 18G2A steel are reported by Sender and Trąmpczyński (1995). In this Section only main results concerning 18G2A and 40H steel are presented and discussed.

To search the influence of cyclic amplitude and mean stress on the material cyclic behaviour, several sets of experiments were conducted. In every set, the mean stress was kept constant and the amplitude of the cycle was increased step by step. For a chosen amplitude, the cyclic loading was repeated until one cycle ratchetting strain $\delta\varepsilon_r^p$, recorded in the following cycles, becomes either constant (steady state) or zero (shakedown). Then, higher amplitude (cycling amplitude was increased of 20 MPa for 18G2A steel and 25 MPa

for 40H steel) was applied and the specimen was loaded in cycles until a new steady state was achieved and so on.

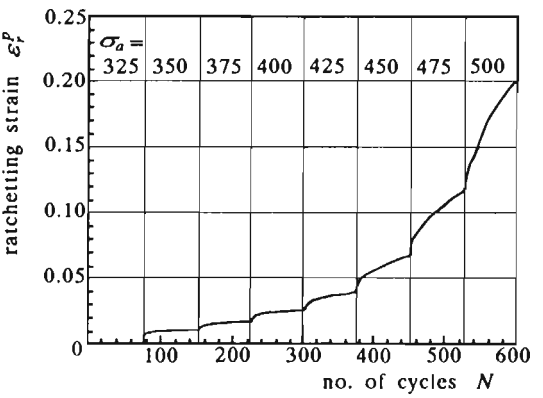

Fig. 11. Ratchetting strain ε_r^p versus the number of cycles for 40H steel cyclic tension-compresion loading with varying amplitudes; $\sigma_m = 500\,\mathrm{MPa}$, $\sigma_a = 325 \div 500\,\mathrm{MPa}$

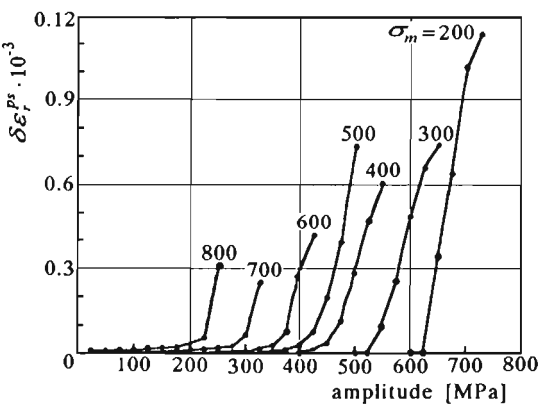

Fig. 12. One-cycle ratchetting steady state strain $\delta\varepsilon_r^{ps}$ versus cyclic amplitude σ_a for 40H steel cyclic tension-compresion loading, with different mean stresses and growing cyclic amplitudes

Results of such an experimental program for mean stress $\sigma_m = 500\,\mathrm{MPa}$ in the case of 40H steel are shown in Fig.11, as the diagram of ratchetting strain ε_r^p versus the number of cycles.

Similar tests were performed for different mean stress and the data concerning one-cycle ratchetting strain $(\delta\varepsilon_r^{ps})$ at a steady state versus the stress amplitude, are shown in Fig.12 for 40H steel. Three types of material behaviour can be distinguished (Fig.13 and Fig.14): I – no ratchetting, II – ratchetting

shakedown and III – ratchetting, what is quite important from engineering point of view.

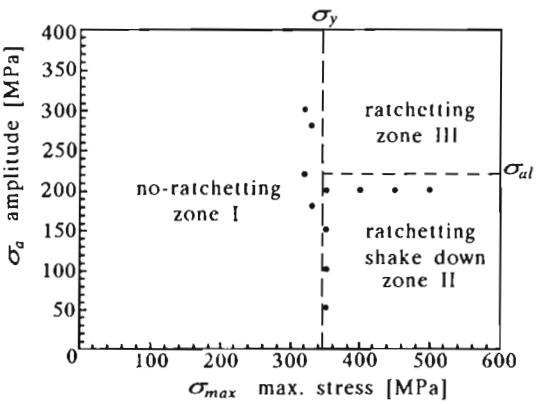

Fig. 13. 18G2A steel ratchetting behavior zones

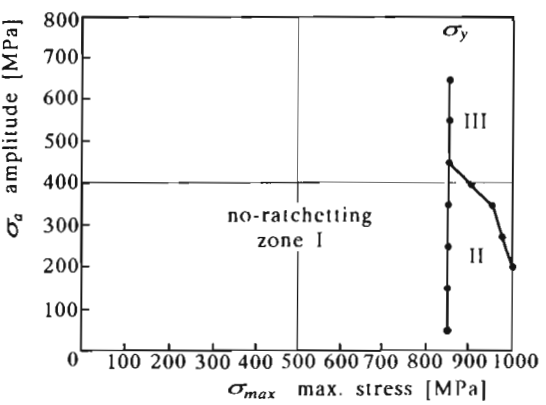

Fig. 14. 40H steel ratchetting behavior zones

In the case of stress-controlled 18G2A cyclic loading (Fig.13), material ratchetting behaviour can be determined providing only two parameters: the virgin material yield value (σ_Y) and the bounding amplitude (σ_{al}). For maximal stress below the yield limit $\sigma_{\max} < \sigma_Y$ only no-ratchetting behaviour is observed. In the case when $\sigma_{\max} \geq \sigma_Y$, two kinds of behaviour can be expected: ratchetting for $\sigma_a > \sigma_{al}$ and ratchetting shakedown for $\sigma_a \leq \sigma_{al}$ (except of $\sigma_m = 0$, when ratchetting effect does not occur in any case).

In the case of 40H steel behaviour (Fig.14) also three zones can be determined. For maximal stress below the yield limit $\sigma_{\max} < \sigma_Y$ only no-ratchetting behaviour is observed. In the case when $\sigma_{\max} \geq \sigma_Y$, two kinds of behaviour can be expected: ratchetting and ratchetting shakedown. Bounding relations for this zones are more complicated than for 18G2A steel.

The results presented in Fig.11 ÷ Fig.14 were obtained using a step-by-step approach (constant mean stress σ_m and increasing amplitude σ_a) on one specimen. Experimental results for 18G2A steel show (cf Sender and Trąmpczyński (1995)) that cyclic loading with smaller amplitudes has no influence on material behaviour with higher amplitudes and strong memory effect of cyclic loading with higher amplitudes on the material behaviour under cyclic loading with smaller amplitude. This memory effect is manifested by a substantial reduction of the ratchetting strain rate. A different behaviour, concerning the influence of smaller amplitudes on material behaviour with higher amplitudes, shows 40H steel (Fig.15).

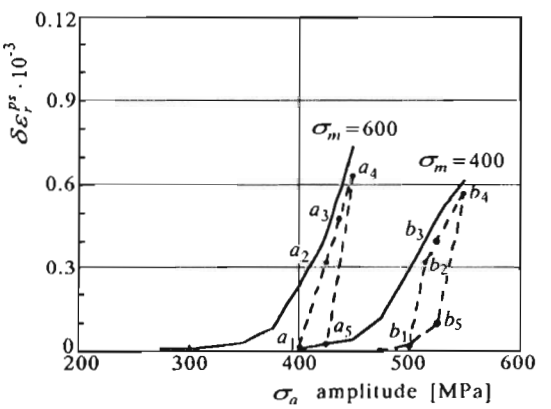

Fig. 15. 40H steel one-cycle ratchetting steady state strain $\delta\varepsilon_r^{ps}$ versus cyclic amplitude for cyclic tension-compresion with constant mean stress $\sigma_m = 600$ MPa and $\sigma_m = 400$ MPa and varying cyclic amplitude σ_a; — results for stepwise growing amplitudes (Fig.12); *-*-* results for the following amplitudes; (a) – $\sigma_m = 600$ MPa, $\sigma_a = 400, 425, 438, 450, 438$ MPa; (b) – $\sigma_m = 400$ MPa, $\sigma_a = 500, 515, 525, 550, 525$ MPa

Results for two levels of mean stress $\sigma_m = 600$ MPa and $\sigma_m = 400$ MPa and five following cyclic amplitudes are presented in Fig.15 (asterisks; a_1-a_2-a_3-a_4-a_5; b_1-b_2-b_3-b_4-b_5) and compared with that for step-wise loading (solid line). The virgin specimen was first loaded with $\sigma_m = 600$ MPa (and $\sigma_m = 400$ MPa) by the amplitude represented by the point $a_1(\sigma_a = 400$ MPa) and $b_1(\sigma_a = 500$ MPa), respectively. When the steady

state was achieved, the cyclic amplitude was increased in a step way to the amplitude represented by the points $a_2(\sigma_a = 425\,\mathrm{MPa})$, $a_3(\sigma_a = 438\,\mathrm{MPa})$, $a_4(\sigma_a = 450\,\mathrm{MPa})$ (and $b_2(\sigma_a = 515\,\mathrm{MPa})$, $b_3(\sigma_a = 525\,\mathrm{MPa})$, $b_4(\sigma_a = 550\,\mathrm{MPa})$ – dashed line) and then decreased to $a_5(\sigma_a = 438\,\mathrm{MPa})$ and $b_5(\sigma_a = 525\,\mathrm{MPa})$.

It is seen, that although the one-cycle ratchetting strain $(\delta\varepsilon_r^{ps})$ at a steady state for the first amplitude (points a_1 and b_1) does not coincide with that for step-wise loading, points for following amplitudes coincide with this line quite well. It means that cyclic loading with smaller amplitudes has influence on material behaviour with higher amplitudes but only in the case of virgin material.

Discrepancy between points a_3 and a_5 (b_3 and b_5), when the amplitude diminishes, indicates the influence of the cyclic loading history with higher amplitudes on the material behaviour under cyclic loading with smaller amplitudes. The resulting one-cycle ratchetting strain at steady state $\delta\varepsilon_r^{ps}$ is much lower than that for the virgin material (compare points 2 and 5 – the ratchetting differs more than 300%).

4. Conclusions

Results concerning monotonic loading, strain controlled symmetric cyclic loading and stress-controlled non-symmetric cyclic loading for 18G2A, St3s, 40H and 45 at room temperature are presented, discussed and compared. Basic qualitative effects detected for 18G2A steel Sender and Trąmpczyński (1995) are confirmed also for different materials. There were defined also some differences in material behaviour and conclusions listed below can be drawn up:

- In the case of monotonic loading, the parameter π_1, shows similar qualitative behaviour and continually increases its value.

  In the case of 18G2A and St3s steel, the parameter Y_1 initially decreases, then increases and saturates at plastic strains $\varepsilon_x^p \approx 0.1$. Further material hardening is caused by increasing the π_1 value only.

  In the case of 40H and 45 steel, the parameter Y_1 continually decreases.

  In all cases, within the yield knee range two simultaneous processes are observed: increase of parameter π_1 and decrease of parameter Y_1.

- The general shape of the π_1 path during cyclic loading (strain-controlled) is established during the first full cycle, and then it changes only slightly to reach a stable loop. The shape of this loop is similar to that of the stress-strain loop (Y_1 =const).

- For all the materials, tested in this experimental program, cyclic loading history (strain-controlled) with smaller amplitudes has no influence on the material cyclic behaviour with higher amplitudes.

- Influence of the cyclic history (strain-controlled) with higher amplitudes on the subsequent cyclic behaviour with smaller amplitudes (memory of maximum prestress which manifests as higher skeleton points values for 18G2A and St3s steel and lower skeleton points for 40H and 45 steel) is observed in the π_1 parameter behaviour in the case of 18G2A steel and in the π_1 and Y_1 parameter behaviour in the case of St3s, 40H and 45 steel.

- Proportional cyclic loading (strain-controlled) after plastic prestrain leads to relaxation of π_1 mainly in the prestrain direction. In the opposite direction the shape of π_1 curve remains almost unchanged right from the very beginning of the cyclic program. Value of Y_1 relaxes symmetrically.

  When quite large uniaxial prestrain (9.2%) is followed by comparatively small cyclic loading amplitudes, the steady state cyclic curve remains unsymmetrical. Such material memory is included in the behaviour of the parameter π_1. In the case of comparatively high cyclic amplitudes, such memory can be almost erased and steady state cyclic curve becomes symmetrical.

- Influence of even complex plastic prestrain history, on following monotonic loading, can be described only by π_1 and Y_1 values resulted from the former history.

- In stress-controlled cyclic limits, material cyclic behaviour described as ratchetting, ratchetting shakedown and no-ratchetting can be referred to certain fields in amplitude versus maximal stress co-ordinates.

  The materials show a strong memory of the cyclic history with higher stress amplitudes on the subsequent cyclic behaviour (ratchetting) with smaller amplitudes.

  In the case of 18G2A steel, cyclic loading history with smaller amplitudes has no influence on the material cyclic behaviour with higher amplitudes.

The 40H steel shows a memory of the cyclic history with smaller stress amplitudes on the subsequent cyclic behaviour (ratchetting) with higher amplitudes.

Acknowledgments

The authors acknowledge support of the State Committee for Scientific Research under Project 3 P 404 031 04.

References

1. BENALLAL A., MARQUIS D., 1987, An Experimental Investigation of Cyclic Hardening of 316 Stainless steel under Complex Multiaxial Loadings, *Trans. of 9th SMIRT Conf.*, **L**, 345-356

2. CHABOCHE J.L., 1975, Viscoplastic Constitutive Equations for the Description for Cyclic and Anisotropic Behaviour of Metals, *Bull. Polish. Acad. Sci., Serie Techn. Sci.*, **23**, 33-42

3. HASSAN T., CORONA E., KYRIAKIDES S., 1992, Ratcheting in Cyclic Plasticity, Part II: Multiaxial Behavior, *I. Journ. of Plasticity*, **8**, 117-146

4. HASSAN T., KYRIAKIDES S., 1992, Ratcheting in Cyclic Plasticity, Part I: Uniaxial Behavior, *I. Journ. of Plasticity*, **8**, 91-116

5. ISHIKAWA H., SASAKI K., 1989, Stress Strain Relations of SUS304 Stainless steel After Cyclic Preloading, *Journ. of Eng. Mat. and Techn.*, **III**, 417-423

6. JHANSALE H., 1975, A New Parameter for the Hysteresis Stress-Strain Behavior of Metals, *ASME Journal of Engineering Materials and Technology*, **97**, 33

7. KOWALEWSKI Z., ŚLIWOWSKI M., SOCHA G., 1994, Określanie cyklicznych właściwości stali 18G2A na podstawie krzywych szkieletowych dla płaskiego stanu naprężenia, *Prace IPPT*, 32/94

8. LANDGRAF R., MORROW J., ENDO T., 1969, Determination of Cyclic Stress-Strain Curve, *Journal of Materials*, **4**, 176

9. LEHMANN TH., RANIECKI B., TRĄMPCZYŃSKI W., 1985, The Bauschinger Effect in Cyclic Plasticity, *Arch. Mech.*, **37**, 6, 643-659

10. OHASHI Y., KAWAI M., KAITO T., 1985, Inelastic Behavior of Type 316 Stainless steel, *J.Eng.Mat.Techn., ASME*, **111**, 278-285

11. OHNAMI M., SAKANE M., NISHINO S., 1988, Cyclic Behavior of Type 304 Stainless steel in Biaxial Stress States at Elevated Temperatures, *Int.J.of Plasticity*, **4**, 77-89

12. RODZIK P., 1993, Plastic Deformation in the Case of Cyclic Loading, Ph.D. Thesis – in polish, 1993

13. SENDER E., JARZĘBOWSKI A., TRĄMPCZYŃSKI W., 1995, The Theoretical Prediction of the Evolution of Kinematic and Isotropic Hardening in the Case of Complex Uniaxial Loading, *Proceedings Plasticity 95 Symposium*

14. SENDER E., TRĄMPCZYŃSKI W., 1995, The 18G2A Steel (Construction steel) Cyclic Behaviour in the Case of Complex Uuniaxial Loading, *Eng. Trans,* **43**, 1-2, 327

15. ŚLIWOWSKI M., 1979, Behavior of Stress-Strain Diagrams for Cyclic Loading, *Bull. of the Polish Acad. of Sciences, Serie Sci. Tech.*, **27**, 115-123

16. TRĄMPCZYŃSKI W., 1989, On a Simple Experimental Technique for the Yield Surface Determination, *Bull. of the Polish Acad. of Sciences, Serie Sci. Tech.*, **37**, 7-12, 407-418

Ewolucja kinematycznego i izotropowego wzmocnienia dla złożonych historii obciążenia jednoosiowego

Streszczenie

W pracy przedstawiono wyniki badań doświadczalnych zachowania się czterech typów stali konstrukcyjnej przy złożonych historiach obciążenia jednoosiowego w zakresie plastycznym. Próbki okrągle, wykonane ze stali 18G2A, St3s, 40H i 45 (dwie pierwsze stale wykazują wzmocnienie cykliczne a dwie ostatnie oslabione), poddawano obciążeniom monotonicznym, cyklicznym dla cykli symetrycznych w odkształceniach oraz cyklicznym dla cykli niesymetrycznych w naprężeniach, w temperaturze pokojowej.

Wykorzystując "dwupunktową" technikę pomiaru powierzchni plastyczności śledzono ewolucję położenia dwóch, dobrze zdefiniowanych, punktów tej powierzchni.

W przypadku powierzchni Hubera-Misesa dane te pozwalają na określenie ewolucji kinematycznego i izotropowego wzmocnienia, którą to ewolucję przedstawiono *w niniejszej pracy dla wyżej wymienionej historii obciążenia jednoosiowego* (rozciąganie-ściskanie).

Manuscript received June 19, 1995; accepted for print December 19, 1995